

Quantum Phases in Resonantly Driven Fermi Hubbard Model

Ning Sun,¹ Pengfei Zhang,¹ and Hui Zhai^{1,2}

¹*Institute for Advanced Study, Tsinghua University, Beijing, 100084, China*

²*Collaborative Innovation Center of Quantum Matter, Beijing, 100084, China*

(Dated: April 25, 2022)

In this letter we consider quantum phases and the phase diagram of a Fermi Hubbard model under periodic driving that has been realized in recent cold atom experiments, in particular, when the driving frequency is resonant with the interaction energy. The effective Hamiltonian describing this situation contains a correlated hopping term where the density occupation strongly modifies the hopping strength. Focusing on half filling, in addition to the charge and spin density wave phases, large regions of ferromagnetic phase and phase separation are discovered in the weakly interacting regime. The mechanism of this ferromagnetism is attributed to the correlated hopping because in this regime the hopping strength within a ferromagnetic domain is normalized to a larger value than the hopping strength across the domain. Thus, the kinetic energy favors a large ferromagnetic domain and consequently drives the system into a ferromagnetic phase. We note that this is a different mechanism in contrast to the well-known Stoner mechanism for ferromagnetism where the ferromagnetism is driven by interaction energy.

PACS numbers:

Recently, with the help of quantum gas microscope for fermions [1–6], tremendous experimental progresses have been made on quantum simulation of the Fermi Hubbard model. These progresses include the observation of equilibrium properties such as short-range antiferromagnetic correlations [7–9], hidden antiferromagnetic correlations [10], incommensurate spin correlations [11], canted antiferromagnetic correlations [12] and pairing correlations [13] in several different circumstances. In particular, the antiferromagnetic long-range order has been successfully observed through entropy engineering [14]. These progresses also include the study of non-equilibrium transport behaviors such as the measurement of optical conductivity [15], and the spin and charge transport behavior in the strongly interacting regime [16, 17].

Studying Fermi Hubbard model with cold atoms also allows us to open up new avenue beyond the traditional condensed matter paradigm. One of such examples is the periodically driven Fermi Hubbard model [18, 19]. Since the typical parameters of a Hubbard model is the hopping strength J and the on-site interaction U , who are both of the order of electron volt in strongly correlated solid-state materials, it is therefore hard to drive a solid-state material with frequency resonant with these two energy scales. However, in cold-atom optical lattice realization of the Fermi Hubbard model, the typical energy scales for these two parameters are both of the order of thousand Hertz, and it is quite easy to drive the optical lattices with such a frequency. When the driving frequency is resonant with the interaction parameter U , the driving can strongly modify the Fermi Hubbard model. As observed in a recent experiment from the ETH group, the short-range antiferromagnetic correlation can be reduced, or enhanced, or even switch sign to become ferromagnetic correlation [20]. Similar experiment has also been performed by driving the Hubbard model with two-photon Raman transition [21]. Hence, by combining such a resonant driving with the quantum gas microscope, it is very promising to study novel phases induced by periodic

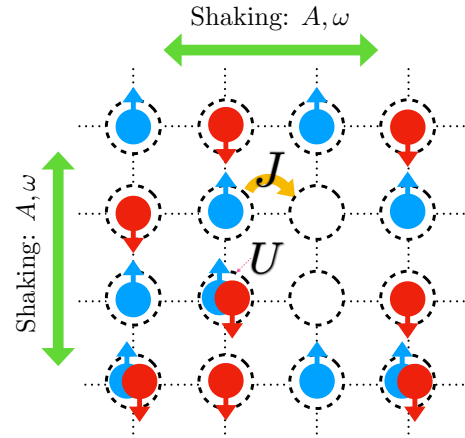


FIG. 1: A schematic of the Fermi Hubbard model on a two-dimensional square lattice. J denotes the hopping strength. U is the on-site interaction. The system is time-periodically modulated by shaking the lattice in a sinusoidal way with frequency ω and amplitude A . Arrows indicate the direction of shaking. Balls with different colors and arrows indicate fermions with different spins.

driving that cannot be accessed in a static system. The goal of this letter is therefore to predict quantum phases and phase diagram of the resonant driven Fermi Hubbard model that is newly realized in cold atom experiments.

Model. We consider a two-dimensional square lattice under similar driving as realized in experiments [20, 28]. The lattice is periodically modulated along the \hat{x} and \hat{y} directions with a frequency ω and an amplitude A , whose single particle Hamiltonian can be written as

$$\hat{H}_0(t) = \frac{\mathbf{p}^2}{2m} + \hat{V}(\mathbf{x} + A \cos(\omega t), \mathbf{y} + A \cos(\omega t)) \quad (1)$$

where m is the mass of an atom. We can now perform a unitary transformation [22]

$$\hat{U}(t) = \exp(-i\mathbf{r} \cdot \mathbf{p}_0(t)) \exp(i\mathbf{p} \cdot \mathbf{r}_0(t)), \quad (2)$$

where $\mathbf{r}_0(t) = -A \cos(\omega t)(1, 1)$ and $\mathbf{p}_0(t) = m\omega A \sin(\omega t)(1, 1)$ are both two-dimensional vectors. This unitary transformation first transfers position $\mathbf{r}_0(t)$ into the comoving frame where the lattice becomes static but an extra time-dependent gauge field is introduced, and subsequently it shifts the momentum $\mathbf{p}_0(t)$ to remove the gauge field by introducing a time-dependent potential instead. The resulting Hamiltonian is written as

$$\hat{H}_0(t) = \frac{\mathbf{p}^2}{2m} + \hat{V}(\mathbf{r}) + m\omega^2 A \cos(\omega t)(x + y). \quad (3)$$

In principle, the Hamiltonian Eq. 3 is equivalent to the one Eq. 1. Whereas here we choose to start with Eq. 3 instead of Eq. 1 because the time-periodic term is directly coupled to density in Eq. 3. It will be convenient for dealing with the situation where the driving frequency is resonant with the density-density interaction energy.

Now we consider a single-band tight-binding model with the nearest neighboring tunneling coefficient J and on-site Hubbard interaction strength U . The Hamiltonian in a second quantized form is therefore written as

$$\begin{aligned} \hat{H}(t) = & -J \sum_{\substack{\langle i,j \rangle \\ \sigma=\uparrow,\downarrow}} \hat{c}_i^\dagger \hat{c}_j + U \sum_i \left(\hat{n}_{i\uparrow} - \frac{1}{2} \right) \left(\hat{n}_{i\downarrow} - \frac{1}{2} \right) \\ & + \sum_{i,\sigma} f_i(t) \left(\hat{n}_{i\sigma} - \frac{1}{2} \right). \end{aligned} \quad (4)$$

where $\hat{c}_{i\sigma}$ ($\hat{c}_{i\sigma}^\dagger$) is the fermionic annihilation (creation) operator on site i with spin σ , $\hat{n}_{i\sigma}$ is the density operator on site i with spin σ , $\langle \dots \rangle$ denotes the nearest neighboring sites, and $f_i(t) = m\omega^2 A \cos(\omega t)(x_i + y_i)$ with x_i and y_i being the position of the i th lattice site. Throughout this work we focus on the half-filling case and the chemical potential is set to zero.

The last term in the Hamiltonian Eq. 4 can be further gauged away by applying following unitary rotation

$$\hat{R}(t) = \exp(i \sum_{j\sigma} F_j(t) \hat{n}_{j\sigma}), \quad (5)$$

where $F_j(t) = \int^\tau f_j(\tau) d\tau$. Since the tunneling Hamiltonian does not commute with $\hat{n}_{j\sigma}$, this transformation will modify the tunneling Hamiltonian. If the modulation frequency ω is the largest energy scale of the problem, one can make a high-frequency expansion to obtain an effective time-independent Hamiltonian [23, 24]. To the lowest order, the effective Hamiltonian takes the same form as the normal Hubbard model and the only modification is that the tunneling coefficient is renormalized as $\tilde{J} = J\mathcal{B}_0(\mathcal{A})$, where we use \mathcal{B}_l to denote the l th Bessel function and $\mathcal{A} = m\omega d$ is the normalized shaking amplitude hereinafter. d is the distance of two Wannier wave packets in the nearest neighboring lattice sites.

However, this expansion falls down when the modulation frequency ω , or l th multiple of it, is comparable to one of the energy scale of the problem, say, the Hubbard interaction strength U . That is to say, $l\hbar\omega \approx U$, and we call it the l th

resonance. Note that in this case, because $U - l\hbar\omega$ is a small energy scale, we should apply another unitary transformation

$$\hat{R}(t) = \exp(i \sum_j \omega t \hat{n}_{j\uparrow} \hat{n}_{j\downarrow}) \exp(i \sum_{j\sigma} F_j(t) \hat{n}_{j\sigma}), \quad (6)$$

which first alters the interaction strength to an effective one $\tilde{U} = U - l\hbar\omega$. Then the high frequency expansion can be safely applied, and to the lowest order it again results in a time-independent effective Hamiltonian written as

$$\hat{H}_{\text{eff}} = \sum_{\langle i,j \rangle, \sigma} -\tilde{J}_{\text{eff},\sigma}^{(ij)} \hat{c}_{i\sigma}^\dagger \hat{c}_{j\sigma} + \tilde{U} \sum_i \left(\hat{n}_{i\uparrow} - \frac{1}{2} \right) \left(\hat{n}_{i\downarrow} - \frac{1}{2} \right). \quad (7)$$

Here $\tilde{J}_{\text{eff},\sigma}^{(ij)}$ is defined as

$$\tilde{J}_{\text{eff},\sigma}^{(ij)} = J_0 \hat{a}_{ij\bar{\sigma}} + J_1 \hat{b}_{ij\bar{\sigma}}, \quad (8)$$

and it is the effective hopping amplitude, where $\bar{\sigma}$ denotes the complement of σ , $J_0 = J\mathcal{B}_0(\mathcal{A})$, $J_1 = J\mathcal{B}_l(\eta_{ij}\mathcal{A})$ ($\eta_{ij} = \pm 1$ for $(i_x, i_y) = (j_x \pm 1, j_y)$ or $(i_x, i_y) = (j_x, j_y \pm 1)$), and

$$\hat{a}_{ij\sigma} = (1 - \hat{n}_{i\sigma})(1 - \hat{n}_{j\sigma}) + \hat{n}_{i\sigma} \hat{n}_{j\sigma}, \quad (9)$$

$$\hat{b}_{ij\sigma} = (-1)^l (1 - \hat{n}_{i\sigma}) \hat{n}_{j\sigma} + \hat{n}_{i\sigma} (1 - \hat{n}_{j\sigma}). \quad (10)$$

In above, the site dependence of J_1 is made implicitly. Note, however, that for even l the Bessel function \mathcal{B}_l is an even function, in which case η_{ij} can be simply dropped and J_1 becomes a constant. Below we will analyse the quantum phases and the corresponding phase diagram of this effective Hamiltonian Eq. 7. Setting J_0 as the energy unit, the phase diagram is controlled by two parameters of J_1/J_0 and \tilde{U}/J_0 , both of which can be easily tuned from positive to negative via control of ω and A .

Symmetry. Before we discuss how to solve this effective Hamiltonian, let us first comment on the symmetry of this problem. Note that the original Hubbard model possesses a SO(4) symmetry [25], which is composed of a spin SU(2), generated by $\hat{S}_z = (1/2) \sum_i \hat{c}_{i\uparrow}^\dagger \hat{c}_{i\uparrow} - \hat{c}_{i\downarrow}^\dagger \hat{c}_{i\downarrow}$, $\hat{S}_+ = \sum_i \hat{c}_{i\uparrow}^\dagger \hat{c}_{i\downarrow}$ and $\hat{S}_- = \hat{S}_+^\dagger$, and a charge SU(2), generated by $\hat{L}_z = -(1/2) \sum_i \hat{c}_{i\uparrow}^\dagger \hat{c}_{i\uparrow} + \hat{c}_{i\downarrow}^\dagger \hat{c}_{i\downarrow} + N_s/2$, $\hat{L}_+ = \sum_i (-1)^i \hat{c}_{i\uparrow}^\dagger \hat{c}_{i\downarrow}$ and $\hat{L}_- = \hat{L}_+^\dagger$. N_s is the total number of sites. The spin SU(2) ensures that the direction of spin-density-wave (SDW) order parameter can be taken along any direction, while the charge SU(2) ensures the degeneracy of a charge-density-wave (CDW) order and the fermion pairing order (P).

In the presence of periodic modulation, considering the time-dependent Hamiltonian Eq. 4, it is straightforward to show that the spin SU(2) symmetry stays, yet the charge SU(2) symmetry no longer holds because \hat{L}_z does not commute with the $\sum_{i,\sigma} f_i(t) \hat{n}_{i\sigma}$ term. However, considering the time-independent effective Hamiltonian Eq. 7, one can show that the charge SU(2) symmetry is recovered for even l case though not for odd l case [26]. Hereafter we focus only on the even l case which possesses the same SO(4) symmetry as the original Hubbard model. In addition, the effective Hamiltonian also possesses particle-hole symmetry at half-filling.

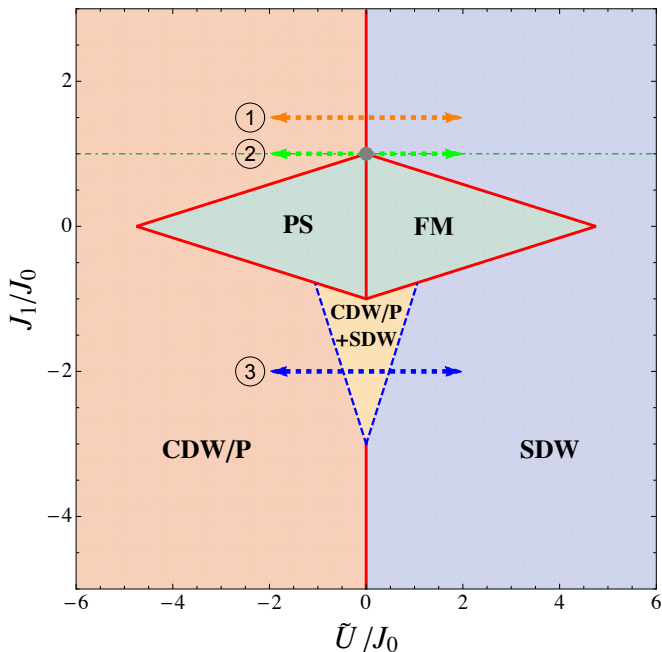


FIG. 2: Phase diagram for the effective Hamiltonian Eq. 7 of a resonantly driven Fermi Hubbard model with even l at half filling. The phase diagram is controlled by two dimensionless parameters, J_1/J_0 and \tilde{U}/J_0 . “CDW” and “SDW” denote charge and spin density wave order. “P” denote fermion pairing order. “FM” denotes ferromagnetism, “PS” denotes phase separation into high and low density regimes. Red lines denote the first order transition and the blue dashes lines denote the second order transition. Dashed arrows mark the lines along which the order parameters are plotted in FIG. 3.

Phase Diagram. We present our results on the phase diagram following from a standard mean-field treatment [26], which is known to be qualitatively reliable for a normal Hubbard model [27]. Thanks to the SO(4) symmetry, we can choose SDW along \hat{z} direction (i.e. $s_i = \langle \hat{n}_{i\uparrow} - \hat{n}_{i\downarrow} \rangle$) and CDW (i.e. $c_i = \langle \hat{n}_{i\uparrow} + \hat{n}_{i\downarrow} \rangle - 1$) as the order parameters in our mean-field theory. Note that when we obtain the CDW order, it means that the system can have either CDW order or fermion pairing order, or an arbitrary combination of them, as the order parameter of the degenerate ground states. Higher order effect will break the degeneracy between CDW and fermion pairing order, but it is beyond the scope of current work.

The phase diagram is shown in Fig. 2. First of all, note that when $J_1/J_0 = 1$, because $\hat{a}_{i\uparrow\sigma} + \hat{b}_{i\downarrow\sigma} = \hat{I}$, the kinetic energy term becomes $-J_0 \sum_{\langle ij \rangle, \sigma} \hat{c}_{i\sigma}^\dagger \hat{c}_{j\sigma}$ and the Hamiltonian recovers the usual Hubbard model. In this case (labeled by 2 in Fig. 2), the result for the normal Hubbard model is retrieved where we obtain a CDW order of (π, π) with attractive interaction ($\tilde{U} < 0$) and a SDW order of (π, π) with repulsive interaction ($\tilde{U} > 0$). Explicitly, the order parameters are chosen as $s_i = (-1)^{i_x+i_y} s$ and $c_i = (-1)^{i_x+i_y} c$, and $s(c)$ gradually vanishes as \tilde{U} approaches zero from the positive (negative) side. As a result, a second order phase transition occur at $\tilde{U} = 0$ (gray dot in FIG. 2). This can be seen from the order parameters plotted

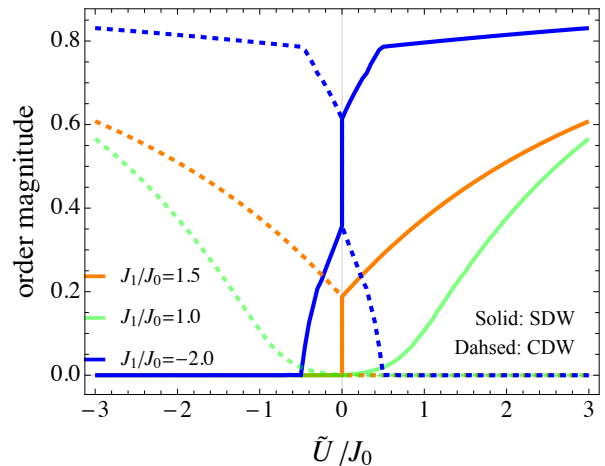


FIG. 3: The CDW order parameter c (dashed lines) and the SDW order parameter s (solid lines) as a function of \tilde{U} for three representative cases labeled as 1-3 in Fig. 2, with $J_1/J_0 = 1.5, 1.0$ and -2.0 , respectively.

as a function of \tilde{U} , shown as green curves in Fig. 3.

Since both CDW and SDW are ordered phases, it requires fine tuning to access a second order transition between them, for which case the hopping parameters has to be fine tuned to $J_1/J_0 = 1$. In another word, when $J_1/J_0 \neq 1$, the more generic situation should be either a first order transition or a phase co-existence regime in between. As marked by the red solid lines in Fig. 2, the phase boundary of CDW and SDW at large $|J_1/J_0|$ is a first order transition. The order parameters are shown with orange lines in Fig. 3 for a representative case (labeled by 1 in Fig. 2), where the CDW or SDW order parameter jumps from a finite value to zero at $\tilde{U} = 0$. At certain regime of J_1/J_0 , a CDW and SDW co-existence regime shows up in between as displayed by the yellow regime in Fig. 2. The order parameters are shown with blue lines in Fig. 3 for a representative case (labeled by 3 in Fig. 2).

The most notable feature in Fig. 2 is the green region. In this region a mean-field ansatz of CDW or SDW orders with ordering vector at (π, π) may not yield any ordered solution. However, when we consider the case of enlarged $2 \times 2, 3 \times 3$, up to $L \times L$ domains, and within each domain the CDW and SDW order parameters are uniformly chosen as c and s while in its neighboring domain they are taken as $-c$ and $-s$, the mean-field ansatz does yield ordered solutions. It can be seen from Fig. 4 which shows that the mean-field ground state energy decreases monotonically as L increases. It indicates that the ground state will form large domains with opposite order parameter values. Moreover, minimizing ground state energy yields $c = 0$ and $s \neq 0$ at positive \tilde{U} and $c \neq 0$ and $s = 0$ at negative \tilde{U} . Hence, the system at positive \tilde{U} possesses spin order, and the increasing of the domain size means the decreasing of the spin ordering wave vector. Eventually, the wave vector decreases toward zero, and the ground state becomes a ferromagnetic state. In another word, as the domain size becomes larger and larger, the system is essentially made

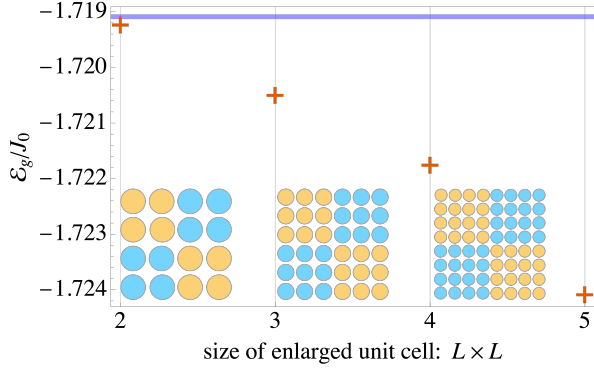


FIG. 4: The mean-field ground state energy as a function of the domain size L . The insets show the configuration for 2×2 , 3×3 and 4×4 blocks where the CDW and SDW order parameters are uniformly distributed within a domain and take opposite values between neighboring domains. For comparison, the solid line is the mean-field energy when order parameters are all zero.

of ferromagnetic domains. For negative \tilde{U} the system tends to phase separation with high density in one domain and low density in its neighboring domain. The transition between the ferromagnetic phase to the SDW phase, as well as the transition from phase separation to CDW, is a first order transition.

It should be emphasized that both the ferromagnetism and the phase separation regime occur at small \tilde{U} . In fact, it is purely due to the correlated hopping effect in the effective Hamiltonian Eq. 7, which originates essentially from the resonant driving. Considering the mean-field configurations as shown in the insets of Fig. 4, let us look at the mean-field value of the effective hopping strength $\langle \hat{J}_{\text{eff},\sigma}^{(ij)} \rangle$ which quantifies how the particle occupations affect the hopping strength and thus affect the bandwidth. We define $J_{\text{eff},\sigma}^{\text{intra}}$ as $\langle \hat{J}_{\text{eff},\sigma}^{(ij)} \rangle$ with both i and j in the same domain, and $J_{\text{eff},\sigma}^{\text{inter}}$ as $\langle \hat{J}_{\text{eff},\sigma}^{(ij)} \rangle$ with i and j across two neighboring domains. It is straightforward to write down both $J_{\text{eff},\sigma}^{\text{intra}}$ and $J_{\text{eff},\sigma}^{\text{inter}}$ as

$$J_{\text{eff},\sigma}^{\text{intra}} = \frac{1}{2} (J_0[1 + (c \mp s)^2] + J_1[1 - (c \mp s)^2]), \quad (11)$$

$$J_{\text{eff},\sigma}^{\text{inter}} = \frac{1}{2} (J_0[1 - (c \mp s)^2] + J_1[1 + (c \mp s)^2]), \quad (12)$$

where \mp corresponds to different spin component. One can show that when $|J_1| < |J_0|$, $|J_{\text{eff},\sigma}^{\text{inter}}|$ is always smaller than $|J_{\text{eff},\sigma}^{\text{intra}}|$. Hence, the size of the domain tends to increase such that there are more intra-domain links than inter-domain links, and therefore the effective bandwidth on average becomes larger. For a given filling, a larger bandwidth leads to more kinetic energy gain. $|J_1| < |J_0|$ is precisely the regime where we find ferromagnetism or phase separation in the phase diagram of Fig. 3 with arbitrary weak interaction. This regime can be easily accessed when \mathcal{A} is small.

It is also illustrative to consider a uniform system with $\tilde{U} = 0$, where the Hamiltonian contains only the correlated tunneling term. Substitute $\hat{J}_{\text{eff},\sigma}^{(ij)}$ by its mean-field value, it is straightforward to compute the kinetic energy of this uniform

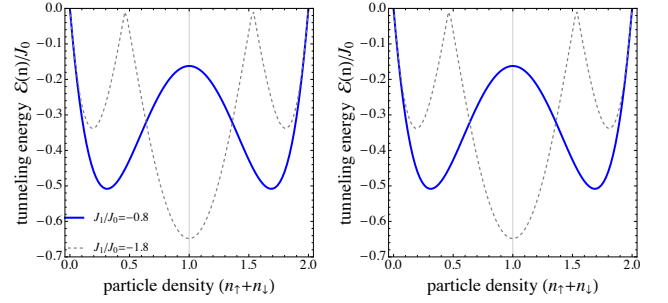


FIG. 5: The mean-field energy with $\tilde{U} = 0$ (a) as a function of total density n with $s_z = 0$ fixed, and (b) as a function of s_z with $n = 1$ fixed. Solid line is for $J_1/J_0 = -0.8$ and the dashed line is for $J_1/J_0 = -1.8$.

system that depends on $n_{i\uparrow}$ and $n_{i\downarrow}$, where $n_{\uparrow} = (n + s_z)/2$ and $n_{\downarrow} = (n - s_z)/2$. We plot the kinetic energy as a function of n for $s_z = 0$ in Fig. 5(a) and as a function of s_z for $n = 1$ in Fig. 5(b) for two representative cases with $J_1/J_0 = -0.8$ and -1.8 . One can see from Fig. 5(a) that for $J_1/J_0 = -0.8$, there are two local minima with one at $n > 1$ and the other at $n < 1$, who locate symmetrically on two sides of $n = 1$, while for $J_1/J_0 = -1.8$ there is only one minimum located at $n = 1$. Similarly, in Fig. 5(b) for $J_1/J_0 = -0.8$, there are two local minima with one at positive s_z and the other at negative s_z , symmetrically distributed around $s_z = 0$, and for $J_1/J_0 = -1.8$ there is only one minimum at $s_z = 0$. Thus, when the system is constrained with the average $n = 1$ and $s_z = 0$, for the case with $J_1/J_0 = -0.8$, it will actually phase separate into domains with either different n or different s_z . The choice is made by the sign of \tilde{U} when a small but finite \tilde{U} perturbation is turned on.

Conclusion and Outlook. The most significant finding of this work is to provide an alternative mechanism for the onset of ferromagnetism in the model with correlated hopping, which roots in the cooperation between the spin order and the correlated hopping. It is driven by the kinetic energy term, and occurs in the weakly interacting regime. This is in contrast to the well-known Stoner ferromagnetism mechanism which is driven by large interaction energy and occurs when the interaction strength is beyond certain critical value. This is also different from the ferromagnetism due to the super-exchange processes discussed in the experiment of Ref. [20] which requires \tilde{U} to be negative.

Finally we shall comment on the experimental observation of this ferromagnetism. First of all, the system itself has been realized with cold atoms, and moreover, a very recent experiment shows that the heating is insignificant in the presence of driving and the life time of the system can be about one second [28]. Second, because this ferromagnetism is driven by kinetic energy, and as one can see from Fig. 5, the energy gain is of the order of bandwidth, thus one expects this ferromagnetism to be observed when temperature is of the order of bandwidth, which can be accessed now by cold atom ex-

periments. Thirdly, the quantum gas microscope techniques mentioned at the beginning can be used to detect real space ferromagnetic domains. Hence, it is quite promising to verify this theory experimentally in very near future.

Acknowledgment. This work is supported MOST under Grant No. 2016YFA0301600 and NSFC Grant No. 11734010.

-
- [1] E. Haller, J. Hudson, A. Kelly, D. A. Cotta, B. Peaudecerf, G. D. Bruce and S. Kuhr, *Single-atom imaging of fermions in a quantum-gas microscope*, Nature Physics **11**, 738 (2015).
- [2] L. W. Cheuk, M. A. Nichols, M. Okan, T. Gersdorf, V. V. Ramasesh, W. S. Bakr, T. Lompe, and M. W. Zwierlein, *Quantum-Gas Microscope for Fermionic Atoms*, Phys. Rev. Lett. **114**, 193001 (2015).
- [3] G. J. A. Edge, R. Anderson, D. Jervis, D. C. McKay, R. Day, S. Trotzky, and J. H. Thywissen, *Imaging and addressing of individual fermionic atoms in an optical lattice*, Phys. Rev. A **92**, 063406 (2015).
- [4] A. Omran, M. Boll, T. A. Hilker, K. Kleinlein, G. Salomon, I. Bloch, and C. Gross, *Microscopic Observation of Pauli Blocking in Degenerate Fermionic Lattice Gases*, Phys. Rev. Lett. **115**, 263001 (2015).
- [5] D. Greif, M. F. Parsons, A. Mazurenko, C. S. Chiu, S. Blatt, F. Huber, G. Ji and M. Greiner, *Site-resolved imaging of a fermionic Mott insulator*, Science **351**, 953-957 (2016).
- [6] L. W. Cheuk, M. A. Nichols, K. R. Lawrence, M. Okan, H. Zhang, and M. W. Zwierlein, *Observation of 2D Fermionic Mott Insulators of 40K with Single-Site Resolution*, Phys. Rev. Lett. **116**, 235301 (2016).
- [7] M. F. Parsons, A. Mazurenko, C. S. Chiu, G. Ji, D. Greif and M. Greiner, *Site-resolved measurement of the spin-correlation function in the Fermi-Hubbard model*, Science **353**, 1253-1256 (2016).
- [8] M. Boll, T. A. Hilker, G. Salomon, A. Omran, J. Nespolo, L. Pollet, I. Bloch and C. Gross, *Spin- and density-resolved microscopy of antiferromagnetic correlations in Fermi-Hubbard chains*, Science **353**, 1257-1260 (2016).
- [9] L. W. Cheuk, M. A. Nichols, K. R. Lawrence, M. Okan, H. Zhang, E. Khatami, N. Trivedi, T. Paiva, M. Rigol and M. W. Zwierlein, *Observation of spatial charge and spin correlations in the 2D Fermi-Hubbard model*, Science **353**, 1260-1264 (2016).
- [10] T. A. Hilker, G. Salomon, F. Grusdt, A. Omran, M. Boll, E. Demler, I. Bloch, C. Gross, *Revealing hidden antiferromagnetic correlations in doped Hubbard chains via string correlators*, Science **357**, 484-487 (2017).
- [11] G. Salomon, J. Koenig, J. Vijayan, T. A. Hilker, J. Nespolo, L. Pollet, I. Bloch, C. Gross, *Direct observation of incommensurate magnetism in Hubbard chains*, arXiv: 1803.08892.
- [12] P. T. Brown, D. Mitra, E. Guardado-Sanchez, P. Schaub, S. S. Kondov, E. Khatami, T. Paiva, N. Trivedi, D. A. Huse and W. S. Bakr, *Spin-imbalance in a 2D Fermi-Hubbard system*, Science **357**, 1385-1388 (2017).
- [13] D. Mitra, P. T. Brown, E. Guardado-Sanchez, S. S. Kondov, T. Devakul, D. A. Huse, P. Schaub and W. S. Bakr, *Quantum gas microscopy of an attractive Fermi-Hubbard system*, Nature Physics **14**, 173 (2018).
- [14] A. Mazurenko, C. S. Chiu, G. Ji, M. F. Parsons, M. Kanasz-Nagy, R. Schmidt, F. Grusdt, E. Demler, D. Greif and M. Greiner, *A cold-atom Fermi-Hubbard antiferromagnet*, Nature **545**, 462-466 (2017).
- [15] R. Anderson, F. Wang, P. Xu, V. Venu, S. Trotzky, F. Chevy, and J. H. Thywissen, *Optical conductivity of a quantum gas*, arXiv:1712.09965.
- [16] M. A. Nichols, L. W. Cheuk, M. Okan, T. R. Hartke, E. Mendez, T. Senthil, E. Khatami, H. Zhang, and M. W. Zwierlein, *Spin Transport in a Mott Insulator of Ultracold Fermions*, arXiv:1802.10018.
- [17] P. T. Brown, D. Mitra, E. Guardado-Sanchez, R. Nourafkan, A. Reymbaut, S. Bergeron, A.-M. S. Tremblay, J. Kokalj, D. A. Huse, P. Schaub, and W. S. Bakr, *Bad metallic transport in a cold atom Fermi-Hubbard system*, arXiv:1802.09456.
- [18] M. Bukov, M. Kolodrubetz and A. Polkovnikov, *Schrieffer-Wolff Transformation for Periodically Driven Systems: Strongly Correlated Systems with Artificial Gauge Fields*, Phys. Rev. Lett. **116**, 125301 (2016).
- [19] A.P. Itin and M.I. Katsnelson, *Effective Hamiltonians for Rapidly Driven Many-Body Lattice Systems: Induced Exchange Interactions and Density-Dependent Hoppings*, Phys. Rev. Lett. **115**, 075301 (2015).
- [20] F. Görg, M. Messer, K. Sandholzer, G. Jotzu, R. Desbuquois and T. Esslinger, *Enhancement and sign change of magnetic correlations in a driven quantum many-body system*, Nature **553**, 481-485 (2018).
- [21] W. Xu, W. Morong, H.-Y. Hui, V. W. Scarola, B. De-Marco, *Correlated Spin-Flip Tunneling in a Fermi Lattice Gas*, arXiv:1711.2061.
- [22] R. Shankar, Principles of Quantum Mechanics, Springer 1994.
- [23] A. Eckardt and E. Anisimovas, *High-frequency approximation for periodically driven quantum systems from a Floquet-space perspective*, New J. Phys **17**, 093039 (2015).
- [24] A. Eckardt, *Colloquium: Atomic quantum gases in periodically driven optical lattices*, Rev. Mod. Phys. **89**, 011004 (2017).
- [25] C. N. Yang and S. C. Zhang, SO_4 symmetry in a Hubbard model, Mod. Phys. Lett. B **4**, 759 (1990).
- [26] Supplementary material for (i) prove the $SO(4)$ symmetry of the effective Hamiltonian for even l , and (ii) describe the mean-field theory.
- [27] N. Nagaosa, Quantum Field Theory in Condensed Matter Physics. Springer 1999.
- [28] M. Messer, K. Sandholzer, F. Gorg, J. Minguzzi, R. Desbuquois, T. Esslinger, *Floquet dynamics in driven Fermi-Hubbard systems*, arXiv:1808.00506.

Supplementary Material: Quantum Phases in Resonantly Driven Fermi Hubbard Model

Ning Sun,¹ Pengfei Zhang,¹ and Hui Zhai^{1,2}

¹Institute for Advanced Study, Tsinghua University, Beijing, 100084, China

²Collaborative Innovation Center of Quantum Matter, Beijing, 100084, China

(Dated: April 25, 2022)

In this supplementary material, we first discuss the symmetry of the resonantly driven Fermi Hubbard model. The SO(4) symmetry [1] of the effective Hamiltonian for even l is proved. Then we establish the mean-field theory adopted in this work for even l , which is consistent with the text-book results [2] for $J_0 = J_1$.

SYMMETRY

In this section we discuss the symmetry of the resonantly driven Fermi Hubbard model. The symmetry is of vital significance since it greatly simplifies the formulation of the mean-field description.

SO(4) symmetry.— A usual bipartite Fermi-Hubbard model, written as $\hat{H} = -J \sum_{\langle i,j \rangle, \sigma} \hat{c}_{i\sigma}^\dagger \hat{c}_{j\sigma} + \tilde{U} \sum_i (\hat{n}_{i\uparrow} - 1/2)(\hat{n}_{i\downarrow} - 1/2)$, possesses SO(4) symmetry [1]. The SO(4) symmetry is resolved into two SU(2) symmetries, the spin SU(2) and the charge SU(2). The generators of spin SU(2) are given by:

$$\hat{S}_z = \frac{1}{2} \sum_i \hat{c}_{i\uparrow}^\dagger \hat{c}_{i\uparrow} - \hat{c}_{i\downarrow} \hat{c}_{i\downarrow}, \quad \hat{S}_+ = \sum_i \hat{c}_{i\uparrow}^\dagger \hat{c}_{i\downarrow}, \quad (1)$$

and

$$\hat{S}_- = \hat{S}_+^\dagger, \quad \hat{S}_x = \frac{\hat{S}_+ + \hat{S}_-}{2}, \quad \hat{S}_y = \frac{\hat{S}_+ - \hat{S}_-}{2i}, \quad (2)$$

who satisfy the commutation relation of the SU(2) algebra. Due to the contraction between spin indices, the very beginning time-dependent Hamiltonian $\hat{H}(t)$ (Eq.(4) in the main text) is invariant under this SU(2) symmetry operations, is also the unitary transformations $\hat{R}(t)$ (Eq.(5) and (6) in the main text). Since the time average does not alter this attribute, one arrives at the conclusion that the effective static Hamiltonian \hat{H}_{eff} in Eq.(7) of the main text also possess this spin SU(2) symmetry no matter l even or odd. This can also be verified directly by checking $[\hat{H}_{\text{eff}}, \hat{S}_\alpha] = 0$ for any $\alpha = x, y, z$. The spin rotational symmetry hence allows us to automatically get a spin-balanced system without any additional magnetic field.

However, regarding the charge SU(2) symmetry, the time-dependent Hamiltonian lacks it for the appearance of the time-dependent onsite energy term (the last term in Eq.(4) of the main text). As a result we do not expect the SO(4) symmetry in general. Nevertheless, it emerges in the effective Hamiltonian with l even. We introduce the charge SU(2) as follows [1].

$$\hat{L}_z = -\frac{1}{2} \sum_i \hat{c}_{i\uparrow}^\dagger \hat{c}_{i\uparrow} + \hat{c}_{i\downarrow}^\dagger \hat{c}_{i\downarrow} + \frac{1}{2} N, \quad (3)$$

$$\hat{L}_+ = \sum_i (-1)^i \hat{c}_{i\uparrow} \hat{c}_{i\downarrow} = \sum_i \exp(i\mathbf{Q} \cdot \mathbf{x}_i) \hat{c}_{i\uparrow} \hat{c}_{i\downarrow} \quad (4)$$

where $\mathbf{Q} = (\pi, \pi)$, N is the total number of lattice sites hereinafter, and

$$\hat{L}_- = \hat{L}_+^\dagger, \quad \hat{L}_x = \frac{\hat{L}_+ + \hat{L}_-}{2}, \quad \hat{L}_y = \frac{\hat{L}_- - \hat{L}_+}{2i}. \quad (5)$$

$\{\hat{L}_z, \hat{L}_x, \hat{L}_y\}$ forms an SU(2) algebra. It can be verified straightforwardly that the effective Hamiltonian \hat{H}_{eff} with l even commutes with all these generators. This fact can also be seen from the following transformation

$$\hat{P} : \hat{c}_{i\uparrow} \rightarrow (-1)^i \hat{c}_{i\uparrow}^\dagger,$$

who maps \hat{H}_{eff} with l even of interaction $+\tilde{U}$ to the same class but of effective interaction $-\tilde{U}$, exchanging the role played by $\{L_i\}$ and $\{S_i\}$. As a result, the spin SU(2) invariance for a model with $-\tilde{U}$ indicates the charge SU(2) symmetry for $+\tilde{U}$. And vice versa. In addition, this transformation also implies the phase diagram should be symmetric under $+\tilde{U} \leftrightarrow -\tilde{U}$ together with the interchange of charge and spin order. However, in the l odd cases, this mapping falls down because of the additional minus sign in $\hat{b}_{i\uparrow\sigma}$.

Particle-hole symmetry.— The half-filled effective Hamiltonian \hat{H}_{eff} holds particle-hole symmetry no matter l even or odd. (i) When l is even, define particle-hole transformation $\hat{C} : \hat{c}_{i\sigma} \rightarrow (-1)^i \hat{c}_{i\sigma}^\dagger$. The Hamiltonian is invariant under \hat{C} : $[\hat{C}, \hat{H}_{\text{eff}}] = 0$. (ii) When l is odd, we further define the bipartite transformation \hat{S} , which switches the A/B sublattices. Then the Hamiltonian is invariant under the combination of \hat{C} and \hat{S} : $[\hat{C}\hat{S}, \hat{H}_{\text{eff}}] = 0$. This symmetry allow us to fix chemical potential $\mu = 0$ during the mean-field calculation at half-filling situation.

MEAN-FIELD TREATMENT

In this section we establish the mean-field theory adopted in this work. As explained in the main text, assuming no canted order, we can consider only the charge density wave (CDW) order and spin density wave (SDW) order in the z direction because of the $SO(4)$ symmetry. We focus on the half-filled spin-balanced system, in which case the total charge density and total magnetic momentum is given by

$$\langle \hat{n} \rangle = 1, \quad \langle \hat{S} \rangle = 0. \quad (6)$$

Path integral approach.— Here we provide a derivation of the mean-field Hamiltonian Eq. (19) via a path integral approach. In the path integral language, the real-time partition function of the system is given by:

$$\begin{aligned} \mathcal{Z} &= \int \mathcal{D}\psi D\bar{\psi} \exp(i \int dt L) \\ L &= \sum_{i,\sigma} i\bar{\psi}_{i\sigma} \partial_t \psi_{i\sigma} + \sum_{\langle i,j \rangle, \sigma} \left(J_0 a_{ij\bar{\sigma}}(\bar{\psi}\psi) + J_1 b_{ij\bar{\sigma}}^l(\bar{\psi}\psi) \right) \bar{\psi}_{i\sigma} \psi_{j\sigma} \\ &\quad - \tilde{U} \sum_i \bar{\psi}_{i\uparrow} \psi_{i\uparrow} \bar{\psi}_{i\downarrow} \psi_{i\downarrow}. \end{aligned} \quad (7)$$

$$(8)$$

Here ψ corresponds to the fermionic field operators, and $a_{ij\bar{\sigma}}$ and $b_{ij\bar{\sigma}}^l$ are given by replacing the operators in $\hat{a}_{ij\bar{\sigma}}$ and $\hat{b}_{ij\bar{\sigma}}^l$ with fields. Since the effective Hamiltonian (Eq. (7) in the main text) contains six-fermion terms, the traditional decoupling based on Hubbard-Stratonovich transformation does not applied directly. However, an alternative way of decoupling based on the similar spirit of Hubbard-Stratonovich transformation should be adopted here. Specifically, by inserting a delta function, we directly introduce the auxiliary bosonic field:

$$\begin{aligned} \mathcal{Z} &= \int \mathcal{D}\psi D\bar{\psi} Dn \prod_{i\sigma} \delta(n_{i,\sigma} - \bar{\psi}_{i,\sigma} \psi_{i,\sigma}) \exp(i \int dt L) \\ L &= \sum_{i,\sigma} i\bar{\psi}_{i\sigma} \partial_t \psi_{i\sigma} + \sum_{\langle i,j \rangle, \sigma} \left(J_0 a_{ij\bar{\sigma}}(n) + J_1 b_{ij\bar{\sigma}}^l(n) \right) \bar{\psi}_{i\sigma} \psi_{j\sigma} \\ &\quad - \tilde{U} \sum_i n_{i\uparrow} n_{i\downarrow}. \end{aligned} \quad (9)$$

$$(10)$$

Thanks to the delta function inserted, one could replace all $\psi^\dagger \psi$ by n in the action. As an equivalence check, if we integrate out n fields first, we get our original action back. Now we introduce another field η to absorb the delta function into an integral:

$$\begin{aligned} \mathcal{Z} &= \int \mathcal{D}\psi D\bar{\psi} Dn D\eta \exp(i \int dt L) \\ L &= \sum_{i,\sigma} i\bar{\psi}_{i\sigma} \partial_t \psi_{i\sigma} + \sum_{\langle i,j \rangle, \sigma} \left(J_0 a_{ij\bar{\sigma}}(n) + J_1 b_{ij\bar{\sigma}}^l(n) \right) \bar{\psi}_{i\sigma} \psi_{j\sigma} \\ &\quad - \tilde{U} \sum_i n_{i\uparrow} n_{i\downarrow} - \sum_{i\sigma} \eta_{i\sigma} (n_{i,\sigma} - \bar{\psi}_{i,\sigma} \psi_{i,\sigma}) \end{aligned} \quad (11)$$

$$(12)$$

As a result, the fermion becomes quadratic. In general, one can integrate out all the fermions to get an effective action of wholly bosonic degrees of freedom. Whereas, the mean-field approximation is to say that all the bosonic fields will be replaced by their saddle point solutions.

Mean-field Hamiltonian.— By doing a Legendre transformation and replacing the fermion bilinears with its expectation values, we obtain the mean-field Hamiltonian

$$\hat{H} = \sum_{\langle i,j \rangle, \sigma} - \left(J_0 a_{ij\bar{\sigma}}(n) + J_1 b_{ij\bar{\sigma}}^l(n) \right) \hat{\psi}_{i\sigma}^\dagger \hat{\psi}_{j\sigma} + \tilde{U} \sum_i n_{i\uparrow} n_{i\downarrow} + \sum_{i\sigma} \eta_{i\sigma} (n_{i,\sigma} - \hat{\psi}_{i,\sigma}^\dagger \hat{\psi}_{i,\sigma}) \quad (13)$$

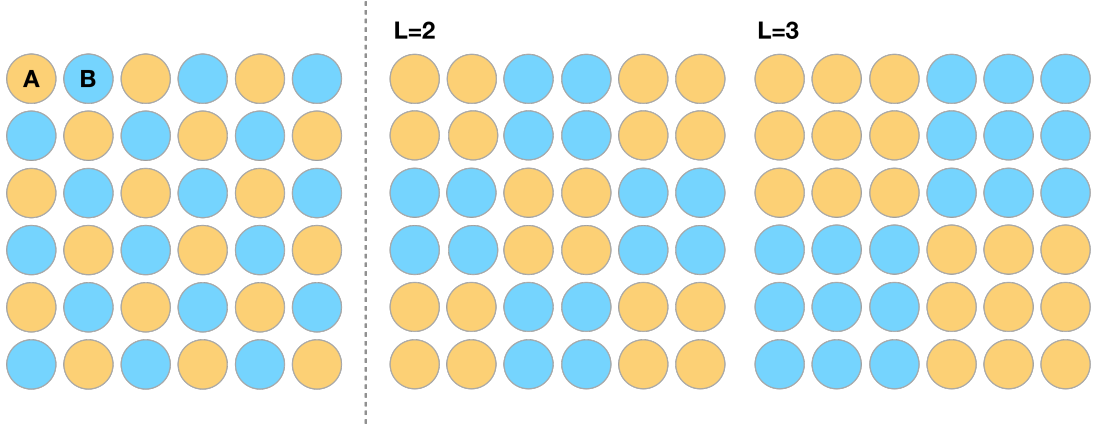


FIG. 1: Schematic of the two cases. Left panel: case 1. Right panel: typical examples of case 2 when $L = 2$ and $L = 3$, respectively, as labeled. Lattice sites of the same color have the same local particle density c_i and local spin density s_i .

where the following replacement is carried out:

$$\hat{a}_{ij\sigma} = (1 - \hat{n}_{i\sigma})(1 - \hat{n}_{j\sigma}) + \hat{n}_{i\sigma}\hat{n}_{j\sigma}, \rightarrow (1 - n_{i\sigma})(1 - n_{j\sigma}) + n_{i\sigma}n_{j\sigma} \quad (14)$$

$$\hat{b}_{ij\sigma} = (-1)^l(1 - \hat{n}_{i\sigma})\hat{n}_{j\sigma} + \hat{n}_{i\sigma}(1 - \hat{n}_{j\sigma}) \rightarrow (-1)^l(1 - n_{i\sigma})n_{j\sigma} + n_{i\sigma}(1 - n_{j\sigma}) \quad (15)$$

For the half-filled spin-balanced situation, we focus on the following two cases here. Notice that, in a half-filled spin-balanced system, the local particle density can be expressed in terms of local charge density and local spin density as

$$n_{i\uparrow} = \frac{1}{2}(1 + c_i + s_i), \quad n_{i\downarrow} = \frac{1}{2}(1 + c_i - s_i) \quad (16)$$

where $\sum_i c_i = 0$ and $\sum_i s_i = 0$. The two cases are then:

1. $c_i = (-1)^{i_x+i_y}c, s_i = (-1)^{i_x+i_y}s$
2. $c_i = (-1)^{[i_x/L]+[i_y/L]}c, s_i = (-1)^{[i_x/L]+[i_y/L]}s$

where c and s are CDW and SDW order parameters introduced, and $[x]$ denotes the ceiling function of x . Substituting these two expressions into the original mean-field Hamiltonian Eq.(13) will yield the mean-field Hamiltonian in each case.

Case 1. The first case is actually the (π, π) order, where the lattice is naturally divided into A/B sublattices and the unit cell of the lattice consists of 2 sites, with one from A and the other from B . The schematic is shown in FIG. 1 (Left).

To be specific, we explicit show here the workflow in the first case. By substitution,

$$n_A \equiv \langle \hat{n}_{i \in A} \rangle = 1 + c, \quad s_A \equiv \langle \hat{S}_{i \in A}^z \rangle = s/2, \quad (17)$$

$$n_B \equiv \langle \hat{n}_{i \in B} \rangle = 1 - c, \quad s_B \equiv \langle \hat{S}_{i \in B}^z \rangle = -s/2, \quad (18)$$

and the mean-field Hamiltonian is explicitly written as:

$$\begin{aligned} \hat{H}_{\text{mf}} = & \sum_{\langle i,j \rangle, \sigma} \{-J_0[(1 - n_{A\bar{\sigma}})(1 - n_{B\bar{\sigma}}) + n_{A\bar{\sigma}}n_{B\bar{\sigma}}] - J_1[(1 - n_{A\bar{\sigma}})n_{B\bar{\sigma}} + n_{A\bar{\sigma}}(1 - n_{B\bar{\sigma}})]\} \hat{c}_{i\sigma}^{A\dagger} \hat{c}_{j\sigma}^B + \text{H. C.} + \frac{\tilde{U}N}{2}(n_{A\uparrow}n_{A\downarrow} + n_{B\uparrow}n_{B\downarrow}) \\ & + \eta_c \left[c - \frac{(\hat{n}_{A\uparrow} + \hat{n}_{A\downarrow}) - (\hat{n}_{B\uparrow} + \hat{n}_{B\downarrow})}{2} \right] + \eta_s \left[s - \frac{(\hat{n}_{A\uparrow} - \hat{n}_{A\downarrow}) - (\hat{n}_{B\uparrow} - \hat{n}_{B\downarrow})}{2} \right] \end{aligned} \quad (19)$$

where $\hat{c}_{i\sigma}^A$ ($\hat{c}_{i\sigma}^B$) are the annihilation operators of i site and spin σ on A (B) sublattice, $\hat{n}_{\mu\sigma} = \frac{1}{N/2} \sum_{i \in \mu} \hat{n}_{i\sigma}$, $\mu = A$ or B , and $n_{\mu\sigma} = \langle \hat{n}_{\mu\sigma} \rangle$. Here η_c and η_s are Lagrangian multipliers of the CDW and SDW orders, respectively, who are also variational parameters to optimize the ground-state energy of \hat{H}_{mf} to get a mean-field solution.

After some substitution and simplification, the mean-field Hamiltonian in momentum space is written as

$$\begin{aligned} \hat{H}_{\text{mf}} = & \sum_{\mathbf{k}\sigma} -P_\sigma(c, s)Q(\mathbf{k})\hat{c}_{\mathbf{k}\sigma}^{A\dagger} \hat{c}_{\mathbf{k}\sigma}^B + \text{H.c.} + \frac{\tilde{U}N}{2}(1 + c^2 - s^2) \\ & + \eta_c \left[c - \frac{(\hat{n}_{A\uparrow} + \hat{n}_{A\downarrow}) - (\hat{n}_{B\uparrow} + \hat{n}_{B\downarrow})}{2} \right] + \eta_s \left[s - \frac{(\hat{n}_{A\uparrow} - \hat{n}_{A\downarrow}) - (\hat{n}_{B\uparrow} - \hat{n}_{B\downarrow})}{2} \right] \end{aligned} \quad (20)$$

where $\hat{c}_{\mathbf{k}\sigma}^A$ ($\hat{c}_{\mathbf{k}\sigma}^B$) are the annihilation operators on A (B) sublattice of quasi-momentum \mathbf{k} and spin σ , $Q(\mathbf{k}) = \sum_i \exp(i\mathbf{k} \cdot \mathbf{d}_i)$, $\{\mathbf{d}_i\}$ are the lattice vectors, and

$$P_{\uparrow}(c, s) = \frac{J_0}{2} [1 - (c - s)^2] + \frac{J_1}{2} [1 + (c - s)^2] \quad (21)$$

$$P_{\downarrow}(c, s) = \frac{J_0}{2} [1 - (c + s)^2] + \frac{J_1}{2} [1 + (c + s)^2] \quad (22)$$

The summation of \mathbf{k} in Eq.(20) is over the first Brillouin zone. Minimization the energy for all parameters $\{c, s, \eta_c, \eta_s\}$ yields a set of mean-field equations that is solved by numerical iteration in this work.

Case 2. The second case actually includes a series of circumstances of L being 2, 3, 4, \dots , ∞ . Typical examples of $L = 2$ and $L = 3$ are shown in the right panel of FIG. 1. In this case, for each independent L , doing the similar substitution as above and solving optimization problem in a numerical way returns us a set of self-consistent mean-field solutions in each L . The ground state should be the one with the lowest ground state energy.

FIG. 2, 3, 4, 5 in the main text are based on the mean-field numerics of above two cases.

Check the formulation for $J_0 = J_1$.— Finally, we explain why our mean-field theory reduces to a traditional one appearing in common text books, e.g. [2]. In fact, the P_{σ} in this case is just a constant with no c and s dependence. Thus the variation of c and s yields:

$$\eta_c = -\tilde{U}Nc \quad \eta_s = -\tilde{U}Ns. \quad (23)$$

Using this relation, we see the mean-field Hamiltonian reduces to a familiar one that appears in textbooks [2].

[1] C. N. Yang and S. C. Zhang, *SO₄ symmetry in a Hubbard model*, Mod. Phys. Lett. B **4**, 759 (1990).

[2] A. Altland, and B. D. Simons. Condensed matter field theory, second edition, Cambridge University Press, 2010.